Tuning Single-Molecule Conductance in Metalloporphyrin-based Wires via Supramolecular Interactions

Albert C. Aragonès,[†] Alejandro Martín-Rodríguez, [◊,‡] Arantzazu Gonzalez Campos,[⊥] Daniel Aravena,[#] Núria Aliaga-Alcalde,[⊥,¥] Eliseo Ruiz,[◊,‡*] Ismael Díez-Pérez[†*]

[†]Department of Chemistry, Faculty of Natural & Mathematical Sciences, King's College London, Britannia House, 7 Trinity Street, London SE1 1DB, United Kingdom.
[‡]Institut de Química Teòrica i Computacional, Universitat de Barcelona, Diagonal 645, 08028 Barcelona, Spain
[◊] Departament de Química Inorgànica i Orgànica, Diagonal 645, 08028 Barcelona, Spain
[⊥] CSIC-ICMAB (Institut de Ciència dels Materials de Barcelona) Campus de la Universitat Autònoma de Barcelona, 08193 Bellaterra, Spain.
[¥] ICREA (Institució Catalana de Recerca i Estudis Avançats)
[#] Departamento de Química de los Materiales, Facultad de Química y Biología, Universidad de Santiago de Chile (USACH), Casilla 40, Correo 33, Chile

Nature has developed amazing supramolecular constructs to deliver outstanding charge transport capabilities.[1] Here we are incorporating simple naturally inspired supramolecular interactions via the axial complexation of metalloporphyrins into the formation of a single-molecule wire in a tunneling gap to dissect the resulting electron pathways through the final chemical adduct. We observe that small structural changes in the axial coordinating ligands result in dramatic changes in the transport properties through the metalloporphyrin-based wire. The increased flexibility of a pyridine-4-yl-methanethiol ligand due to an extra methyl group as compared to a more rigid mercaptopyridine linker allows the former to adopt an unexpected highly conductive stacked structure between the two junction electrodes and the metalloporphyrin ring. DFT calculations reveal a molecular junction structure composed of a shifted stack of the three molecular backbones; the two pyridine ligands sandwiching the metalloporphyrin ring, which is stabilized by a combination of the porphyrin metal center coordination to the pyridinic N and the pyridine/porphyrin π–π overlapping. Contrarily, the more rigid mercaptopyridine ligand presents the expected octahedral coordination of the metalloporphyrin metal center, leading to much lower conductance. Furthermore, we show that a forced imposed along the molecular wire axis results in the formation of a rich variety of other extended supramolecular structures between the pyridine linkers and the porphyrin ring spanning the tunneling gap scoring also relatively high conductance values. This works sets an example of the use of supramolecular chemistry in the construction of efficient molecular conduits towards the development of supramolecular electronics, a concept already exploited in natural organisms.

Keywords: Biomolecular Electronics, Supramolecular Electronics, Single-Molecule Junctions, Metalloporphyrins, Density Functional Calculations.

INTRODUCTION

The concept of Supramolecular Electronics arises from a blend of the fields studying organic crystalline systems and conducting polymers.[2] Moreover, in the last decade, new crystal structure information on natural biomolecular wires has revealed how nature exploits supramolecular electronics using arrays of axially coordinated metalloporphyrins to create highly efficient molecular conduits.[1,3] Metalloporphyrins have been extensively studied as molecular wires owing to a number of appealing properties such as high chemical stability and conjugation, modular metal centre and rich supramolecular chemistry.[4–8] Metalloporphyrins have been chemically connected to metal electrodes either by directly lying flat on the metal surfaces via π-orbital interactions between the metal and the porphyrin ring,[9,10] or by covalent metal-molecule attachment through porphyrin ring substituents.[11–16] Although the latter results in a robust, straightforward method to wire oligo-porphyrins between two electrodes, the inclusion of such anchoring scheme precludes the exploitation of other sources of supramolecular interactions that might lead to the formation of more efficient electron pathways already exploited in natural biomolecular systems. We have recently reported a novel way to form highly conductive metalloporphyrin wires by coordinating axial positions of the metalloporphyrin ring allowing to orient the ring plane perpendicularly to the electron pathway (main junction axis).[17–19] This is possible thanks to the highly axial coordinative capability of both metal centre and porphyrin ring to strong Lewis bases. Such axial ligands act as anchoring molecules or *linkers*,[20] mimicking the common natural schemes exploited in the chemistry of photosynthetic and transmembrane electron transport.[1,3,21]

In this contribution, we aim to study how the conductance of a metalloporphyrin-based supramolecular wire can be fine-tuned via structural changes of the axial coordinative ligands. To this aim, we built single-molecule junctions using an STM-break junction approach of a 5,15-diphenylporphyrin with Co^{II} cations (here after called *Co-DPP*) employing functionalized electrodes with two different pyridine compounds as axial coordinative linkers (see Fig. 1); a pyridine-4-yl-

methanethiol (*PyrMT*)[17–19] and a 4-Pyridinethiol (*PyrT*). We show that the slight structural changes in the axial ligands (differing by one methyl group) result in pronounce changes in the dominant supramolecular interactions that lead to the final molecular wire conformation, and ultimately dictates its final transport properties. We bring DFT structural and transport simulations of the Co-DPP wire using the two different axial ligands to help visualizing the most plausible junction configurations in the different studied cases.

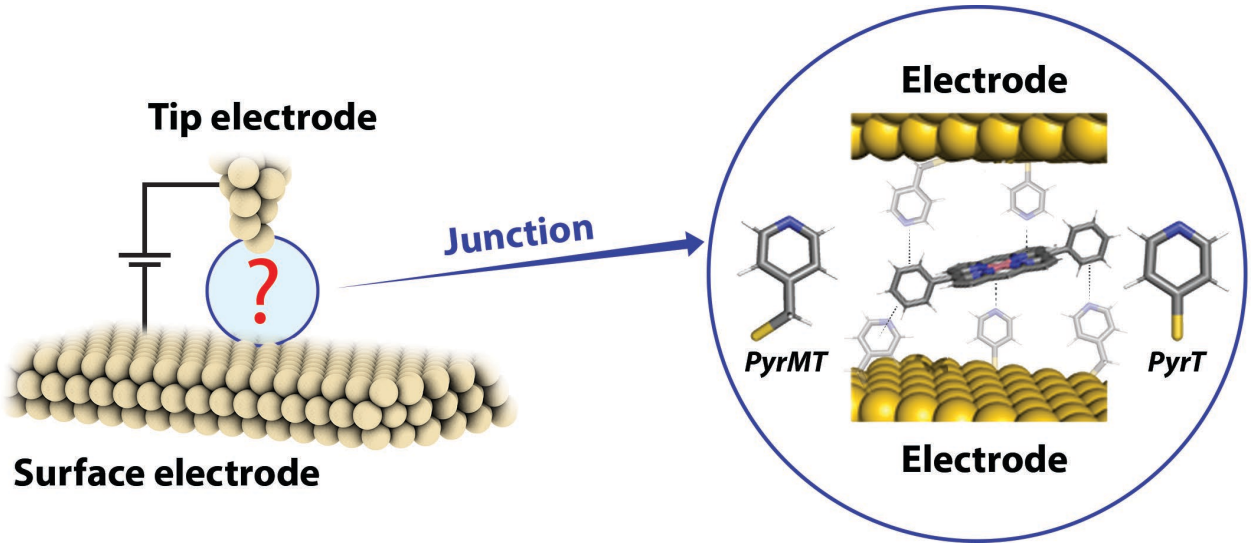

Figure 1. Schematic representation of the supramolecular architecture used to form metalloporphyrin molecular junctions in a STM tunneling gap (left panel) employing pyridine-4-yl-methanethiol *PyrMT* and 4-pyridinethiol *PyrT* linkers (right).

RESULTS AND DISCUSSION

The STM-BJ technique[22,23] was used to form and measure the conductance of individual *Co-DPP* dissolved in an organic medium when they get trapped between the two Au electrodes of a STM junction functionalized with either *PyrMT* or *PyrT* linkers. The electrode functionalization is done *ex-situ* by exposing the electrodes to a solution of each thiolated linker (see preparation and characterization of the functionalized electrodes in Supplementary Information (SI) section 1). We employed the dynamic STM-BJ method, referred as *tapping*,[23] where the STM tip electrode is driven repeatedly in and out of contact with the substrate electrode (see details in SI section 6). During the

retraction cycle, individual *Co-DPP* dissolved in the working media can spontaneously span the electrodes gap forming a transient molecular junction. Characteristic *plateaus*-like features show up in the current versus separation (retraction) curves as a result of the molecular wire breakdown (see representative ones in the Fig. 2 insets).[24,25] Typically, a thousand of retraction curves displaying plateaus features are selected and accumulated in 1D and 2D semi-log conductance histograms (for details see SI sections 2 and 6) resulting in prominent peaks, which provide most probable single-molecule conductance values. Fig. 2a and 2b show the corresponding 1D histograms for *Co-DPP* junctions employing *PyrMT* and *PyrT*, respectively (see corresponding 2D histograms in SI section 2). Both junctions present multiple conductance signatures (peaks I to III) that are attributed to different linker-metalloporphyrin stable geometries as the STM tip is being retracted and gap separation increases. Experiments in the absence of either *Co-DPP* (*PyrMT* and *PyrT* only) or linkers (*Co-DPP* only) show no evident peak features within the same conductance range (see SI section 4.2). Also, *DPP* (metal-free metalloporphyrin) junctions in the presence of both *PyrMT* and *PyrT* show the absence of the highest peak I conductance signature (see SI Section 4.1), which demonstrate that the peak I feature results from the axial coordination with the metal center in both cases, while peaks II and III are the result of pyridine−porphyrin ring interactions.[17] The exact final junction's geometries are, however, unknown. The multiple conductance signatures observed in both cases bring several findings: (i) the more flexible *PyrMT* linker allows a larger number of possible stable junction's geometries, (ii) the geometries achieved with the flexible *PyrMT* linker are two orders of magnitude more conductive than those with the more rigid *PyrT*, and (iii) two electron pathways (through Metal and through porphyrin ring) are present with both linkers.

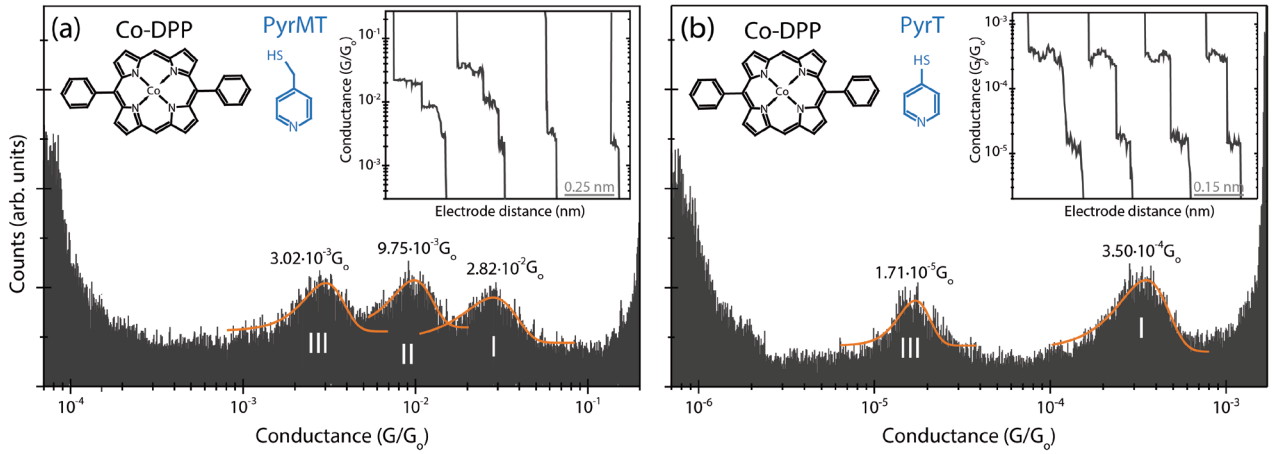

Figure 2. 1D semi-log conductance histograms for the *Co-DPP* junctions using pyridine-4-yl-methanethiol *PyrMT* (a) and 4-pyridinethiol *PyrT* (b) functionalization of both electrodes. The conductance values are extracted from Gaussian fits of the peaks. The insets show representative individual current traces displaying multiple-plateau features used to build the 1D histograms (see 2D histograms in SI section 2). Counts have been normalized versus the total amount of counts. The applied BIAS voltage was set to +7.5 mV.

We have performed DFT calculations (see details in SI section 5) to identify the dominant chemical interactions in the linker/metalloporphyrin/linker junction for the two studied linkers, and deduce plausible geometries related to the observed conductance signatures (peaks I to III in Fig. 2). We had initially proposed an axial coordination scheme for the pyridine linkers standing perpendicular to the porphyrin plane[17,19] (Fig. 1 right), inspired from the crystal structure of similar metal complexes.[26] However, the computed conductance from the transmission function using PBE+U functional for a *Co-DPP* coordinated by two "standing up" *PyrTM* linkers results in a value of ~10^{-6} G_0 (see SI section X), which is several orders of magnitude below the experimental value ($2.82 \cdot 10^{-2}$ G_o). Such discrepancies are too large to be accounted by using a PBE+U functional including corrections for the well-known underestimated highest (lowest) occupied (unoccupied) molecular orbitals (HOMO-LUMO) energy gap in the GGA functionals that usually results in even larger (overestimated) conductance values. We then performed a detailed structural analysis of the most likely geometries of the linker/metalloporphyrin/linker adduct in a constrained tunneling gap. We started by optimizing isolated *PyrMT* and *PyrT* linkers on the electrode surface using a many-body approach to include the

dispersion term. The *PyrMT* shows a much larger propensity to "lie down" on the electrode surface (Fig. 3a), scoring 14.0 kcal/mol more stable than the "standing up" geometry. The *PyrT* linker, on the other hand, computes a much lower 6.0 kcal/mol difference between both conformations, which suggest high likeliness of finding the linker in a "standing up" geometry (Fig. 3b) when forming part of a compact monolayer, as the ones prepared in the experiments (see SI section 6). Moreover, the "standing up" geometry for the *PyrT* linker in a monolayer of the molecule on gold has been previously suggested from STM imaging.[27,28] The DFT optimized structures for the whole linker/*Co-DPP*/linker junction for the two supramolecular wires are shown in Fig. 3c and 3d, and the computed conductance values from the corresponding transmission functions are $6.84 \cdot 10^{-2}$ G_0 and $2.46 \cdot 10^{-4}$ G_0, respectively for the *PyrMT* and *PyrT* junctions, in excellent agreement with the experimental data corresponding to the peak I feature, $2.82 \cdot 10^{-2}$ G_0 and $3.50 \cdot 10^{-4}$ G_0, respectively. The major supramolecular interactions lead in each case to a completely different junction; the *PyrMT* linker forms a π-stacked conformation coordinating the metal center, while the *PyrT* preferably coordinates the metal center in a full standing up fashion. Fig. 3c and d configurations are then ascribed to the most likely molecular wire configurations leading to the peaks I transmissions in Fig. 2a and b. We conclude here that the larger flexibility of the *PyrMT* promotes the stabilization of the final junction structure through π-stacking interactions, while the rigid *PyrT* remains in an orthogonal coordinative geometry. The shorter conduction path in the *PyrMT* junction justifies its larger transmission. It is also important to remark the unusual coordination geometry of the metalloporphyrin with the *PyrMT* ligand, which evidences the interplay between linker-linker neighbor interactions and linker-Au surface interactions (Fig. 3a), the latter stabilizing the observed final "lying down" conformation for the *PyrMT* ligand.

To support the above scenario, we have also performed ellipsometry measurements of a molecular layer of the form linker*/Co-DPP/*linker for both *PyrMT* and *PyrT* linkers on a Au surface (see details in SI Section 1). The resulting thickness values are consistent with the formation of a Au/PyrMT(lying down)/Co-DPP and a Au/PyrT(standing up)/Co-DPP, supporting our hypothesis.

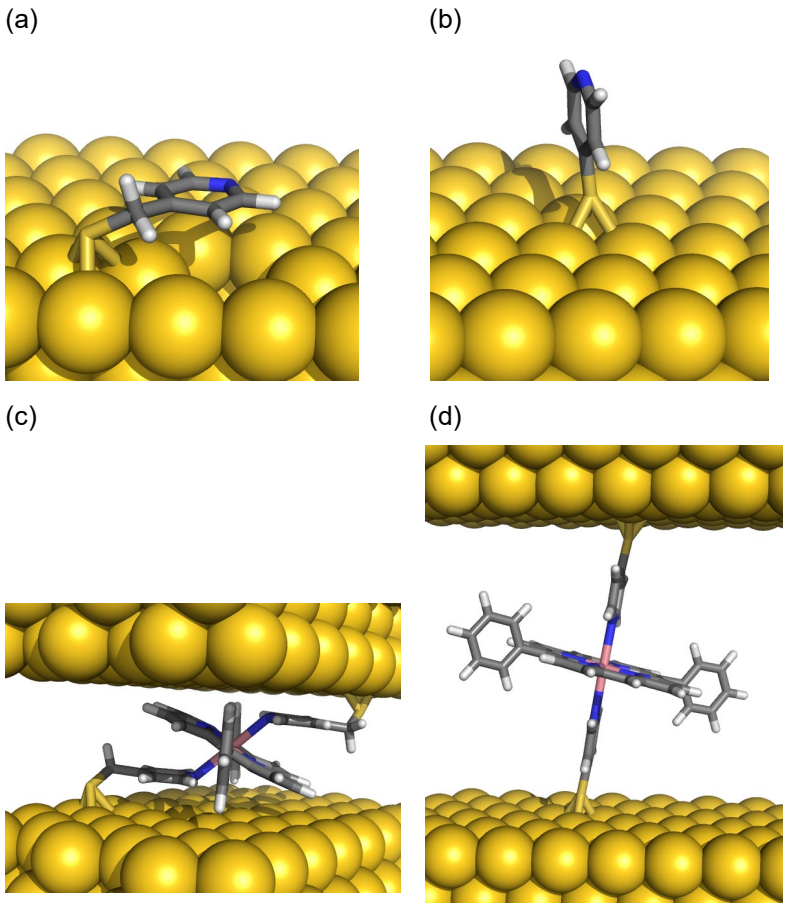

Figure 3. DFT optimized structures for the *PyrMT* (a) and *PyrT* (b) ligands deposited on Au(111). Optimized junction structures attributed to the highest conductance signatures labelled as I in Fig. 2a and 2b., respectively for the *PyrMT* (c) and *PyrT* (d) systems.

We turn now our attention to the conductance features II and III in Figs. 2a and b, originating from interactions between the linkers and the porphyrin ring. To this aim, we first perform additional experiments using a non-substituted porphyrin (*Co-P*) and its metal-free (*P*) homologous (Fig. 4). The *Co-P* junctions using *PyrMT* linkers (Fig. 4a) show two distinguishable molecular conductance signatures at $9.31 \cdot 10^{-3}$ G_0 and $3.01 \cdot 10^{-4}$ G_0. Same experiments with *P* (Fig. 4b) yield a unique low conductance feature at $2.24 \cdot 10^{-4}$ G_0 close to the low conductance observed in Fig. 4a, which leads us to same previous peak assignment: pyridine−metal coordination (signature I) and pyridine−porphyrin backbone (signature II or III). The small discrepancy (~2.3x) in both Co-P and Co-DPP cases (Table I) might be due to the negative inductive effect of the phenyl substituents to the porphyrin ring, which slightly shift the energy of the LUMO frontier orbital closer to the Fermi

level and reduce the energy barrier for the transmitted electrons,29–31 assuming a simple tunneling model with LUMO transport (see PDOS in SI section 5). In addition, the absence of one of the low conductance signatures (II or III) in Fig. 4a when compared to the *Co-DPP* results with the same linker (Fig. 2a) evidences the active role of the phenyl porphyrin substitutions in the formation of the supramolecular junction. This pyridine-phenyl interaction is also confirmed by the same measurements performed on junctions based on a 5,15-dibisphenylporphyrin (*DBPP*), which bears bi-phenyl groups to the porphyrin substitution (see SI section 4.3). The *DBPP* junctions with *PyrMT* linkers display additional conductance signatures (up to 4 overlapping peaks are visible) as compare to the two observed in *DPP* (peaks II and III, SI section 4.1), which demonstrates the additional accessible interaction sites brought by each phenyl ring. At this point, we bring your attention to the summarizing Table I to ease the results comparison among the different supramolecular junctions.

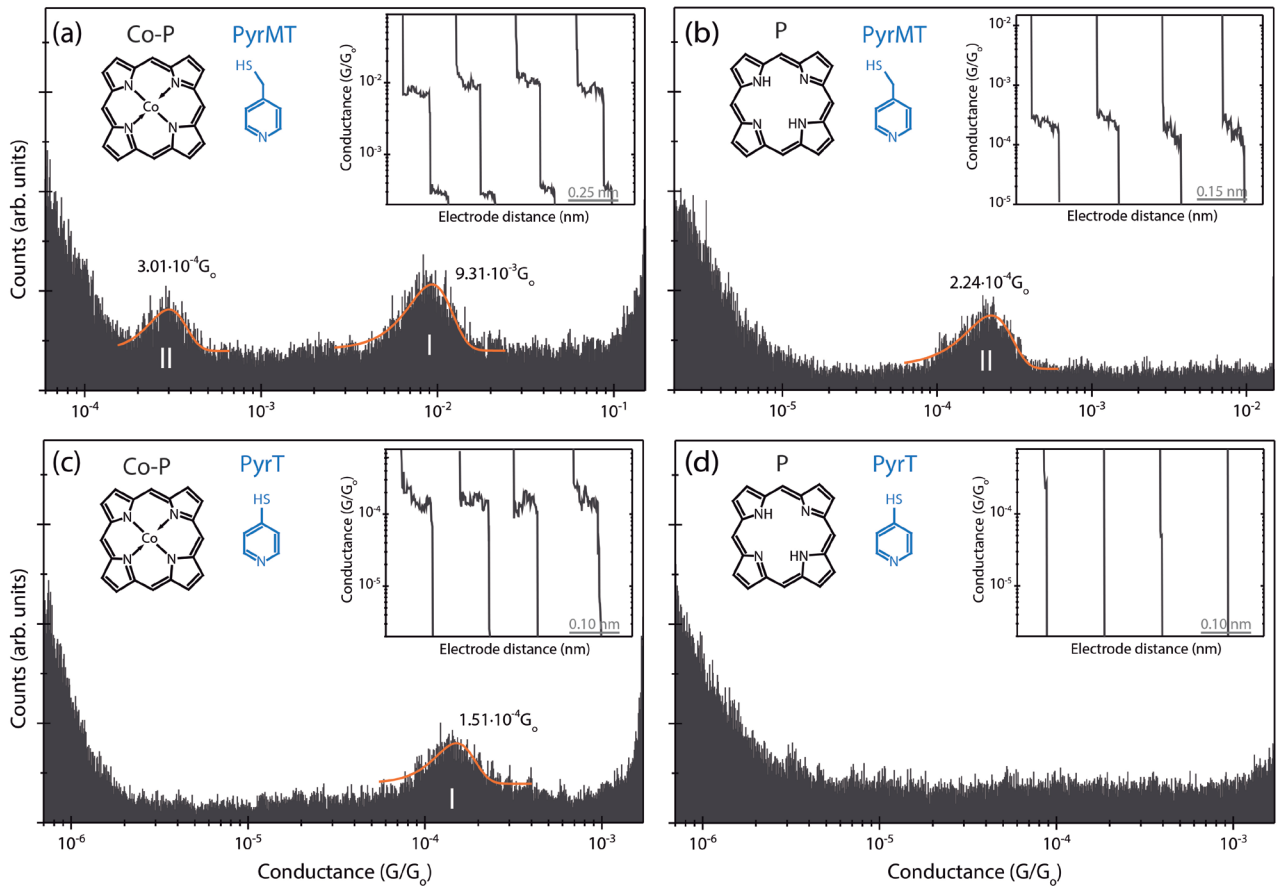

Figure 4. 1D semi-log conductance histograms for the *Co-P* (a,c) and *P* (b,d) molecules employing *PyrMT* (a,b) and *PyrT* (c,d) linkers. The conductance values are extracted from Gaussian fits of the peaks. The insets show representative individual current traces used to build the 1D histograms.

Counts have been normalized versus the total amount of counts. The applied Bias voltages were set to +7.5 mV (a,b,d) and +15 mV (c).

Table I. Summary of conductance values of the different conductance signatures for all porphyrin compounds and linkers combination expressed as $10^{-4}G_o$.

	Porphyrin	*Co-DPP*			*DPP*			*Co-P*			*P*		
Linker	*Peaks*	**I**	**II**	**III**	**I**	**II**	**III**	**I**	**II**	**III**	**I**	**II**	**III**
PyrMT		282	97.5	30.2	-	80.8	23.1	93.1	3.01	-	-	2.24	-
PyrT		3.5	-	0.17	-	-	0.16	1.51	-	-	-	-	-

The *Co-P* junctions employing a *PyrT* linker (Fig. 4c) shows a unique conductance feature whose value is close to the conductance signature I in *Co-DDP* junctions with the same linker (Fig. 2b), and therefore, ascribed to an axial "standing up" coordination of the pyridine to the metal center. The small discrepancy (~2.3x) in both *Co-P* and *Co-DPP* cases (Table I) might be due to the negative inductive effect of the phenyl substituents to the porphyrin ring, which slightly shift the energy of the LUMO frontier orbital closer to the Fermi level and reduce the energy barrier for the transmitted electrons,[29–31] assuming a simple tunneling model with LUMO transport (see PDOS in SI section 5). The absence of conductance signatures II and/or III using *PyrT* linkers (Figs. 4c-d) implies that the enhanced flexibility of the *PyrMT* linker, which presents a conductance signature for the junction with the non-substituted free-metal porphyrin (*P*, Fig. 4b), readily interact with the porphyrin ring thanks to its more accessible π-stacking orientation (Fig. 3a).[24,25] When both the metal center and the phenyl substitutions are removed, the *PyrT* is unable to establish any stable interaction with the porphyrin backbone *P* resulting in a silent conductance histogram (Fig. 4d).

(a) (b)

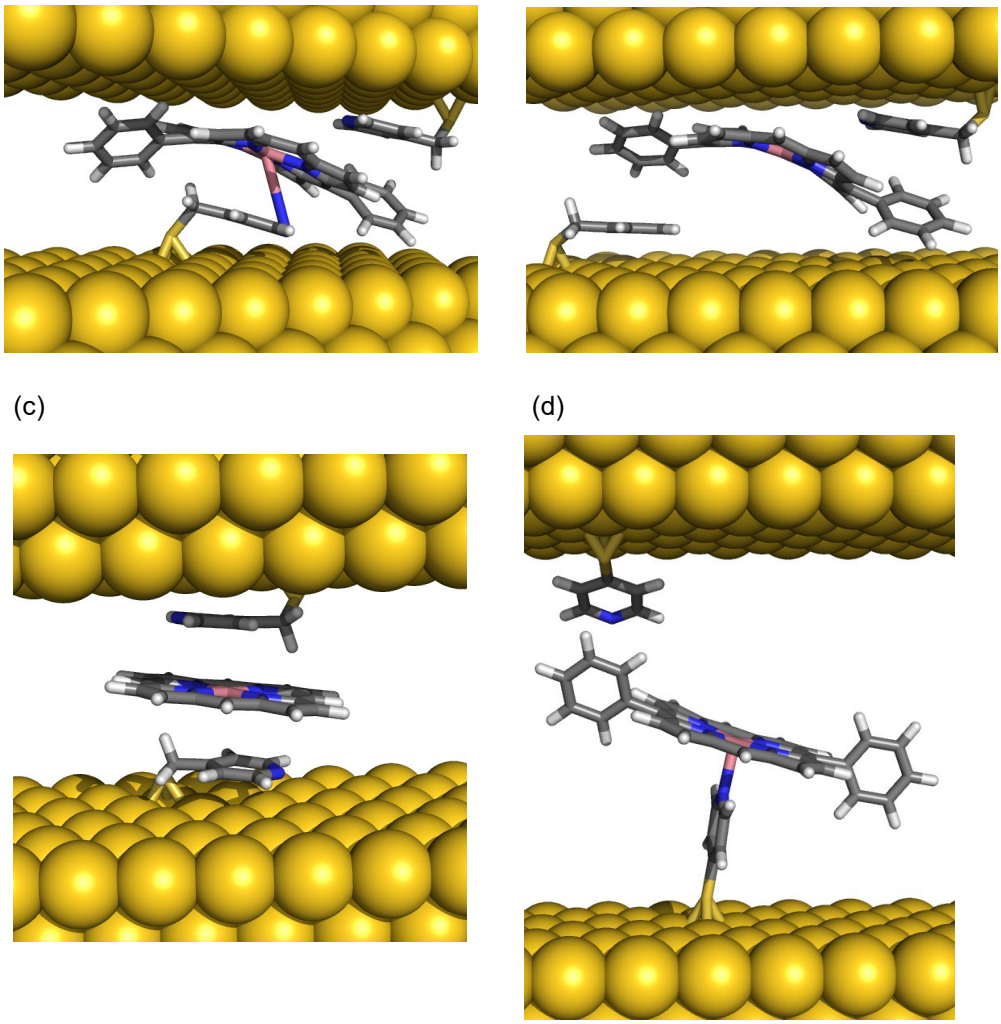

Figure 5. DFT optimized structures for the low conductance signatures of *PyrMT* with *Co-DPP* metalloporphyrin (a and b) labelled as II and I in Fig.2a, lowest conductance signature for the *PyrMT* with *Co-P* labelled as I in Fig.4a (c) and *PyrT* with *Co-DPP* (d) labelled as II in Fig.2b.

We again conducted DFT calculations to analyze the details of the interactions that lead to the observed II and III conductance signatures for the *PyrMT* linker, where the metal is not directly participating in the junction electron pathway. Figure 5 summarizes stable DFT junction configurations whose computed conductance values lie within the range of the experimental ones (other stable configurations whose conductance lied well below the experimental range were not considered). Figures 5a and b shows two stable configurations corresponding to the replacement of one and two *PyrMT*-metal interactions respectively, by *PyrMT*-phenyl interactions in the *Co-DPP*. These interactions arise from the effective π-π stacking between the pyridine moiety of the *PyrMT*

linker and the phenyl substitution of the porphyrin. The calculated conductance values for these two optimized geometries are $6.81 \cdot 10^{-3}$ and $4.50 \cdot 10^{-3}$ G_o in agreement with the experimental values of $9.75 \cdot 10^{-3}$ and $3.02 \cdot 10^{-3}$ G_o (Table I), and they are also consistent with a dynamic picture of consecutive more extended conformations as the junction is elongated during the tip electrode pulling (SI Fig. S3.1) where conformation 5b is able to span a larger electrode-electrode gap separation. In the absence of phenyl substitutions (*Co-P* and *P*), we found effective supramolecular interactions between the pyridine moiety of the *PyrMT* and the two pyrrolic rings of the porphyrin (Fig. 5c). Note that this conformation does not imply interactions with the metal center and that it also seems to be hindered by the presence of the phenyl substitutions in the *Co-DPP* case, where the pyridine-phenyl interaction dominates. The computed conductance of Fig. 5c configuration yields $5.5 \cdot 10^{-4}$ G_o, in good agreement with the experimental value for the *P*/*PyrT* system (Table I). Finally, the optimized geometries for the *Co-DPP/PyrT* system suggest two plausible options where one or two metal-pyridine coordination(s) is(are) replaced by π-π phenyl-pyridine interactions which are enabled thanks to the dihedral rotation of the phenyl substituent (Fig. 5d and e). The calculated conductance values are $4.21 \cdot 10^{-5}$ and $1.37 \cdot 10^{-5}$ G_o, respectively, both close to the corresponding experimental III signature,$1.71 \cdot 10^{-5}$ G_o (Table I). The total DFT energies for both configurations indicate the interaction with two phenyl substituents (Fig. 5e) is 12.6 Kcal/mol more stable suggesting this one as the most plausible scenario for the conductance feature III. This assumption is also supported by the results corresponding to the free-metal *DPP*, where the homologous configuration with two phenyl-pyridine interactions (Fig. S5.6) is also 17.5 Kcal/mol more stable, leading to a calculated conductance of $1.48 \cdot 10^{-5}$ G_o, close to the experimental value of $1.56 \cdot 10^{-5}$ G_o (see Fig. S4.1b). The absence of conductance signatures and the peak II signatures in Fig. 4d and c respectively is then explained by the inability of the *PyrT* linker to stablish effective π-π interactions with the pyrrolic ring.

The summarizing Figure 6 maps out all the supramolecular landscape leading to effective conductance signatures in our porphyrin-based single molecule junctions, visualizing each computed

supramolecular geometry to every observed single molecule conductance feature. Figure 6's picture opens conceptually to new ways of designing nanoscale molecule wires exploiting well-known supramolecular interactions, paving the way to Supramolecular Electronics. We also expect this work to serve as a platform to study charge transport in biological moieties system exploiting very similar supramolecular interactions to produce well-known scenarios of long-range electron transfer.

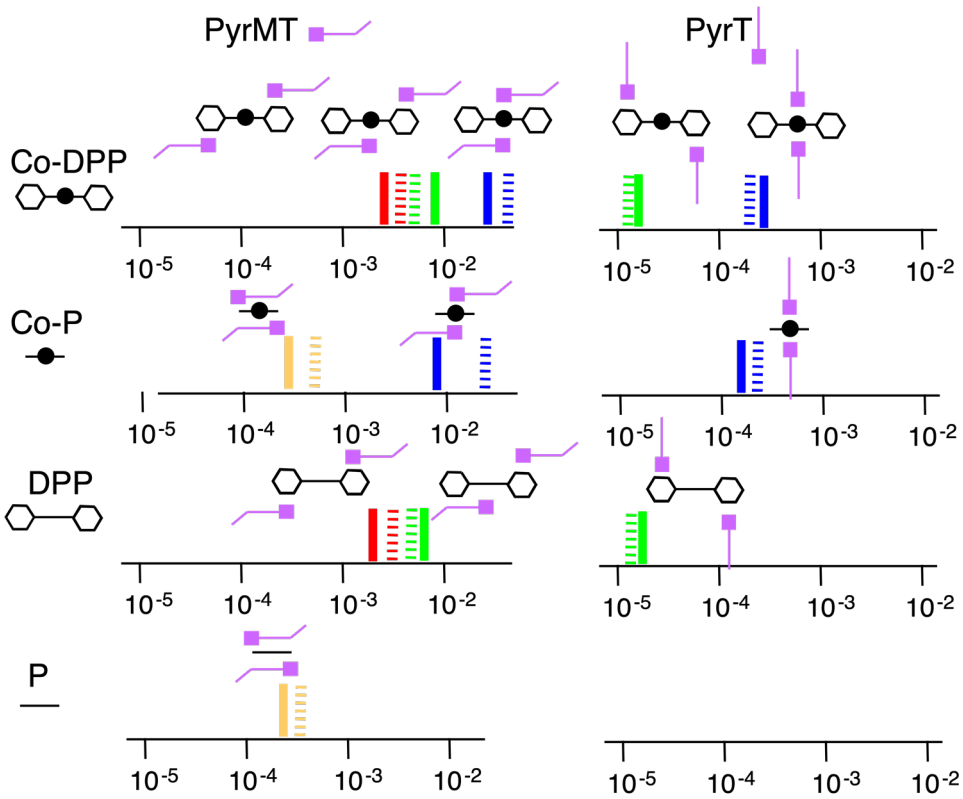

Figure 6. Schematic diagram of the supramolecular landscape for all formed molecular junctions. The conductance values are represented on the X-axis in G_0 units (solid and stripped lines are the experimental and the theoretical values respectively) for both linkers (*PyrMT* and *PyrT*) and the four studied porphyrin systems. Simplified structural models confirmed by DFT are drawn for each conductance signature.

CONCLUSIONS

Concluding, we have studied the formation of single-molecule electrical contacts in a tunneling junction exploiting the rich axial coordination landscape in metalloporphyrin molecular systems using pyrimidine-based linkers. We demonstrate that changes in the linker flexibility result in strikingly different supramolecular interactions between the pyridinic linker and the porphyrin,

leading to completely molecular junction geometry. Briefly summarized in Figure 6, an extra methyl group in a *PyrMT* linker, as compare to a *PyrT* linker, confers extra conformational degrees of freedom to the pyridine group resulting in likely pyridine/porphyrin π-π stacking conformations, as opposed to classical perpendicular axial coordination geometries occurring with the more rigid *PyrT* linker. The supramolecular wires resulting from these two distinct geometries differ by at least an order of magnitude, being the π-π stacking conformations more conductive. As the molecular junction is mechanically stretched, we are able to probe extended supramolecular configurations where either the pyrrolic ring or/and the phenyl side groups of the metalloporphyrin readily provide with additional interacting points to the pyridine linkers, allowing switching to new pathways where the metal center is not involved in the electron transport process across the molecular junction.

These results demonstrate the large conductance tunability of a molecular wire via tweaking its internal supramolecular interactions and present a novel platform to investigate the fascinating, yet unknown, field of the mechanobiology of electron transport in complex biomolecular structures.

EXPERIMENTAL SECTION

Experimental Methods

Computational Methods

Electron transport calculations were carried out with the molecule sandwiched between five Au layers with a 5 x 4 surface unit cell using the Siesta[32] and Gollum[33] codes with the GGA[34]+U functional (U = 4.0 eV) using the exchange-correlation functional proposed by van Voorhis[35] and coworkers to include dispersion effects. The +U approach was employed to have semiquantitative conductance values due to the better description of the energy of the frontier orbitals. A double-ζ basis set with polarization was used combined with pseudopotentials. For Au atoms, two pseudopotentials have been employed 11 e^- pseudopotential for optimizations and $1e^-$ for the transport properties[36]. For the cobalt atoms, a semicore pseudopotential was used, thus, the 3p

orbitals were considered within the basis sets. To obtain the conductance value we approximate $G = T(E_F)G_0$ which should be suitable for very low biases. To compare the PBE results obtained with Siesta and Gollum results against a hybrid functional, the Artaios code was used to calculate the transport properties within the Wide Band Limit (WBL) approximation. The electronic structure was obtained using Gaussian code with the B3LYP functional and the LANL2DZ basis set.

In the case of the optimization of the two ligands (*PyrMT* and *PyrT*) on the Au surface and the comparison of the relative energies for *lying-down* and *standing-up* conformations is a difficult case for pair dispersion models as the van Voorhis functional. Hence, the calculations were performed for the most accurate many-body approach[37] implemented in the FHI-AIMS code[38] using the PBE functional and the tight basis set[39,40]. The structures of the free metal and metalloporphyrins (see for instance, Figs. 3 and 6) interacting axially with the linkers that are necessary for the transport calculations were obtained from DFT structure optimizations using the Siesta code.

ASSOCIATED CONTENT

Supporting Information

The Supporting Information (SI) is available free of charge at XXX

SI content: characterization of functionalized electrodes, 2D conductance maps, pulling curves and plateau length histograms, control single-molecule measurements, theoretical results, technical details of the single-molecule transport measurements, synthesis of compounds

AUTHOR INFORMATION

Corresponding Authors

*ismael.diez_perez@kcl.ac.uk

*eliseo.ruiz@antares.qi.ub.edu

ORCID

Notes

Authors declare no competing financial interest.

ACKNOWLEDGMENTS

The research reported here was supported by the Spanish *Ministerio de Ciencia, Innovación y Universidades* (grants PGC2018-093863-B-C21 and MDM-2017-0767) and the ERC Grant *Fields4CAT* (grant 772391). A.M.R. thanks the same *Ministerio* for a predoctoral FPI grant. E.R. thanks Generalitat de Catalunya for an ICREA Academia award and for the SGR2017-1289 grant. The authors acknowledge the general facilities of the University of Barcelona (CCiT-UB) and the computer resources, technical expertise and assistance provided by the Barcelona Supercomputing Centre.

REFERENCES

(1) Clarke, T. A.; Edwards, M. J.; Gates, A. J.; Hall, A.; White, G. F.; Bradley, J.; Reardon, C. L.; Shi, L.; Beliaev, A. S.; Marshall, M. J.; et al. Structure of a Bacterial Cell Surface Decaheme Electron Conduit. *Proc. Natl. Acad. Sci. U. S. A.* **2011**, *108* (23), 9384–9389.

(2) Meijer, E. W.; Schenning, A. P. H. J. Material Marriage in Electronics. *Nature* **2002**, *419* (6905), 353–354.

(3) Wang, F.; Gu, Y.; O'Brien, J. P.; Yi, S. M.; Yalcin, S. E.; Srikanth, V.; Shen, C.; Vu, D.; Ing, N. L.; Hochbaum, A. I.; et al. Structure of Microbial Nanowires Reveals Stacked Hemes That Transport Electrons over Micrometers. *Cell* **2019**, *177* (2), 361-369.e10.

(4) Liu, Z.-F.; Wei, S.; Yoon, H.; Adak, O.; Ponce, I.; Jiang, Y.; Jang, W.-D.; Campos, L. M.; Venkataraman, L.; Neaton, J. B. Control of Single-Molecule Junction Conductance of Porphyrins via a Transition-Metal Center. *Nano Lett.* **2014**, *14* (9), 5365–5370.

(5) SUSLICK, K. S.; RAKOW, N. A.; KOSAL, M. E.; CHOU, J.-H. The Materials Chemistry of Porphyrins and Metalloporphyrins. *J. Porphyrins Phthalocyanines* **2000**, *04* (04), 407–413.

(6) Mohnani, S.; Bonifazi, D. Supramolecular Architectures of Porphyrins on Surfaces: The Structural Evolution from 1D to 2D to 3D to Devices. *Coord. Chem. Rev.* **2010**, *254* (19), 2342–2362.

(7) Beletskaya, I.; Tyurin, V. S.; Tsivadze, A. Y.; Guilard, R.; Stern, C. Supramolecular Chemistry of Metalloporphyrins. *Chem. Rev.* **2009**, *109* (5), 1659–1713.

(8) Jurow, M.; Schuckman, A. E.; Batteas, J. D.; Drain, C. M. Porphyrins as Molecular Electronic Components of Functional Devices. *Coordination Chemistry Reviews*. 2010, pp 2297–2310.

(9) Perrin, M. L.; Prins, F.; Martin, C. a.; Shaikh, A. J.; Eelkema, R.; van Esch, J. H.; Briza, T.; Kaplanek, R.; Kral, V.; van Ruitenbeek, J. M.; et al. Influence of the Chemical Structure on the Stability and Conductance of Porphyrin Single-Molecule Junctions. *Angew. Chemie* **2011**, *123* (47), 11419–11422.

(10) Perrin, M. L.; Martin, C. A.; Prins, F.; Shaikh, A. J.; Eelkema, R.; van Esch, J. H.; van

Ruitenbeek, J. M.; van der Zant, H. S. J.; Dulić, D. Charge Transport in a Zinc-Porphyrin Single-Molecule Junction. *Beilstein J. Nanotechnol.* **2011**, *2*, 714–719.
(11) Sedghi, G.; Sawada, K.; Esdaile, L. J.; Hoffmann, M.; Anderson, H. L.; Bethell, D.; Haiss, W.; Higgins, S. J.; Nichols, R. J. Single Molecule Conductance of Porphyrin Wires with Ultralow Attenuation. *J. Am. Chem. Soc.* **2008**, *130* (27), 8582–8583.
(12) Sedghi, G.; García-Suárez, V. M.; Esdaile, L. J.; Anderson, H. L.; Lambert, C. J.; Martín, S.; Bethell, D.; Higgins, S. J.; Elliott, M.; Bennett, N.; et al. Long-Range Electron Tunnelling in Oligo-Porphyrin Molecular Wires. *Nat. Nanotechnol.* **2011**, *6* (8), 517–523.
(13) Li, Z.; Smeu, M.; Ratner, M. A.; Borguet, E. Effect of Anchoring Groups on Single Molecule Charge Transport through Porphyrins. *J. Phys. Chem. C* **2013**, *117* (29), 14890–14898.
(14) Li, Z.; Borguet, E. Determining Charge Transport Pathways through Single Porphyrin Molecules Using Scanning Tunneling Microscopy Break Junctions. *J. Am. Chem. Soc.* **2011**, *134* (1), 63–66.
(15) Simbeck, A. J.; Qian, G.; Nayak, S. K.; Wang, G.-C.; Lewis, K. M. Gold–Sulfur Bond Breaking in Zn(II) Tetraphenylporphyrin Molecular Junctions. *Surf. Sci.* **2012**, *606* (17–18), 1412–1415.
(16) El Abbassi, M.; Zwick, P.; Rates, A.; Stefani, D.; Prescimone, A.; Mayor, M.; Van Der Zant, H. S. J.; Dulić, D. Unravelling the Conductance Path through Single-Porphyrin Junctions. *Chem. Sci.* **2019**, *10* (36), 8299–8305.
(17) Aragonès, A. C.; Darwish, N.; Saletra, W. J.; Pérez-García, L.; Sanz, F.; Puigmartí-Luis, J.; Amabilino, D. B.; Díez-Pérez, I. Highly Conductive Single-Molecule Wires with Controlled Orientation by Coordination of Metalloporphyrins. *Nano Lett.* **2014**, *14* (8), 4751–4756.
(18) Ponce, I.; Aragonès, A. C. A. C.; Darwish, N.; Pla-Vilanova, P.; Oñate, R.; Rezende, M. C. M. C.; Zagal, J. H. J. H.; Sanz, F.; Pavez, J.; Díez-Pérez, I. Building Nanoscale Molecular Wires Exploiting Electrocatalytic Interactions. *Electrochim. Acta* **2015**, *179*, 611–617.
(19) Noori, M.; Aragonès, A. C.; Di Palma, G.; Darwish, N.; Bailey, S. W. D.; Al-Galiby, Q.; Grace, I.; Amabilino, D. B.; González-Campo, A.; Díez-Pérez, I.; et al. Tuning the Electrical Conductance of Metalloporphyrin Supramolecular Wires. *Sci. Rep.* **2016**, *6* (1), 37352.
(20) Puigmartí-Luis, J.; Saletra, W. J.; González, A.; Amabilino, D. B.; Pérez-García, L. Bottom-up Assembly of a Surface-Anchored Supramolecular Rotor Enabled Using a Mixed Self-Assembled Monolayer and Pre-Complexed Components. *Chem. Commun. (Camb).* **2014**, *50* (1), 82–84.
(21) Regan, J. J.; Ramirez, B. E.; Winkler, J. R.; Gray, H. B.; Malmström, B. G. Pathways for Electron Tunneling in Cytochrome c Oxidase. *J. Bioenerg. Biomembr.* **1998**, *30* (1), 35–39.
(22) Xu, B.; Tao, N. J. Measurement of Single-Molecule Resistance by Repeated Formation of Molecular Junctions. *Science* **2003**, *301* (5637), 1221–1223.
(23) Aragonès, A. C.; Haworth, N. L.; Darwish, N.; Ciampi, S.; Bloomfield, N. J.; Wallace, G. G.; Diez-Perez, I.; Coote, M. L. Electrostatic Catalysis of a Diels–Alder Reaction. *Nature* **2016**, *531* (7592), 88–91.
(24) Kiguchi, M.; Ohto, T.; Fujii, S.; Sugiyasu, K.; Nakajima, S.; Takeuchi, M.; Nakamura, H. Single Molecular Resistive Switch Obtained via Sliding Multiple Anchoring Points and Varying Effective Wire Length. *J. Am. Chem. Soc.* **2014**, *136* (20), 7327–7332.
(25) Miguel, D.; Álvarez de Cienfuegos, L.; Martín-Lasanta, A.; Morcillo, S. P.; Zotti, L. A.; Leary, E.; Bürkle, M.; Asai, Y.; Jurado, R.; Cárdenas, D. J.; et al. Toward Multiple Conductance Pathways with Heterocycle-Based Oligo(Phenyleneethynylene) Derivatives. *J. Am. Chem. Soc.* **2015**, *137* (43), 13818–13826.
(26) Dey, S.; Ikbal, S. A.; Rath, S. P.; Kirkhouse, J. B.; Kittner, M.; Major, C.; Mchugh, C. J.; Murdoch, P.; Smith, W. E.; Osuka, A.; et al. Self-Assembly of Cobalt(Ii) and Zinc(Ii) Tetranitrooctaethylporphyrin via Bidentate Axial Ligands: Synthesis, Structure, Surface Morphology and Effect of Axial Coordination. *New J. Chem.* **2014**, *38* (4), 1458.

(27) Ramírez, E. A.; Cortés, E.; Rubert, A. A.; Carro, P.; Benítez, G.; Vela, M. E.; Salvarezza, R. C. Complex Surface Chemistry of 4-Mercaptopyridine Self-Assembled Monolayers on Au(111). *Langmuir* **2012**, *28* (17), 6839–6847.
(28) Herrera, S.; Tasca, F.; Williams, F. J.; Calvo, E. J.; Carro, P.; Salvarezza, R. C. Surface Structure of 4-Mercaptopyridine on Au(111): A New Dense Phase. *Langmuir* **2017**, *33* (38), 9565–9572.
(29) Aragonès, A. C.; Darwish, N.; Im, J.; Lim, B.; Choi, J.; Koo, S.; Díez-Pérez, I. Fine-Tuning of Single-Molecule Conductance by Tweaking Both Electronic Structure and Conformation of Side Substituents. *Chem. - A Eur. J. (Weinheim an der Bergstrasse, Ger.* **2015**, *21* (21), 7716–7720.
(30) Xiao, X.; Nagahara, L. A.; Rawlett, A. M.; Tao, N. Electrochemical Gate-Controlled Conductance of Single Oligo(Phenylene Ethynylene)S. *J. Am. Chem. Soc.* **2005**, *127* (25), 9235–9240.
(31) Venkataraman, L.; Park, Y. S.; Whalley, A. C.; Nuckolls, C.; Hybertsen, M. S.; Steigerwald, M. L. Electronics and Chemistry: Varying Single-Molecule Junction Conductance Using Chemical Substituents. *Nano Lett.* **2007**, *7* (2), 502–506.
(32) Soler, J. M.; Artacho, E.; Gale, J. D.; García, A.; Junquera, J.; Ordejón, P.; Sánchez-Portal, D. The SIESTA Method for Ab Initio Order-N Materials Simulation. *J. Phys. Condens. Matter* **2002**, *14* (11), 2745–2779.
(33) Ferrer, J.; Lambert, C. J.; García-Suárez, V. M.; Manrique, D. Z.; Visontai, D.; Oroszlany, L.; Rodríguez-Ferradás, R.; Grace, I.; Bailey, S. W. D.; Gillemot, K.; et al. GOLLUM: A next-Generation Simulation Tool for Electron, Thermal and Spin Transport. *New J. Phys.* **2014**.
(34) Perdew, J. P.; Burke, K.; Ernzerhof, M. Generalized Gradient Approximation Made Simple. *Phys. Rev. Lett.* **1996**, *77* (18), 3865–3868.
(35) Vydrov, O. A.; Van Voorhis, T. Nonlocal van Der Waals Density Functional: The Simpler the Better. *J. Chem. Phys.* **2010**.
(36) Toher, C.; Sanvito, S. Effects of Self-Interaction Corrections on the Transport Properties of Phenyl-Based Molecular Junctions. *Phys. Rev. B* **2008**, *77* (15), 155402.
(37) Ren, X.; Rinke, P.; Blum, V.; Wieferink, J.; Tkatchenko, A.; Sanfilippo, A.; Reuter, K.; Scheffler, M. Resolution-of-Identity Approach to Hartree-Fock, Hybrid Density Functionals, RPA, MP2 and GW with Numeric Atom-Centered Orbital Basis Functions. *New J. Phys.* **2012**.
(38) Blum, V.; Gehrke, R.; Hanke, F.; Havu, P.; Havu, V.; Ren, X.; Reuter, K.; Scheffler, M. Ab Initio Molecular Simulations with Numeric Atom-Centered Orbitals. *Comput. Phys. Commun.* **2009**, *180* (11), 2175–2196.
(39) Jensen, S. R.; Saha, S.; Flores-Livas, J. A.; Huhn, W.; Blum, V.; Goedecker, S.; Frediani, L. The Elephant in the Room of Density Functional Theory Calculations. *J. Phys. Chem. Lett.* **2017**.
(40) Lejaeghere, K.; Bihlmayer, G.; Björkman, T.; Blaha, P.; Blügel, S.; Blum, V.; Caliste, D.; Castelli, I. E.; Clark, S. J.; Dal Corso, A.; et al. Reproducibility in Density Functional Theory Calculations of Solids. *Science (80-.).* **2016**.